Wasit Journal of Engineering Sciences
Journal homepage: https://ejuow.uowasit.edu.iq
Vol. 14 No. 3 September 2026, pp.106-119
https://doi.org/10.31185/ejuow.v14i3.998

ISSN 2305-6932
Original Research

Neural-Fuzzy Controller Design for Left Ventricular Assist Device Speed Regulation

Ruaa F. Rawdan[1], Ekhlas H. Karam[1]
[1]Computer Engineering Department, College of Engineering, Mustansiriyah University, Baghdad, Iraq.

Corresponding Author Email: engruaa09@gmail.com

Received Jul. 29, 2026 Revised Aug. 20, 2026 Accepted Aug. 27, 2026 Online Sep. 1, 2026

ABSTRACT

The mechanical Left Ventricular Assist Device (LVAD) has become an important therapeutic device for patients with advanced heart failure. However, regulating LVAD pump speed under varying physiological conditions remains challenging due to the nonlinear and time-varying nature of the cardiovascular system (CVS). In this study, the CVS is represented using a lumped-parameter state-space model of the left ventricle derived from a nonlinear equivalent circuit. A model-free Neural Network PID (NN-PID) controller integrated with a fuzzy inference system is proposed for LVAD speed regulation. The NN-PID controller enables model-free pump speed control, while the fuzzy inference system adaptively tunes the controller parameters to accommodate changes in physiological conditions. Simulation results demonstrate that the proposed NN-PID controller improves pump-flow tracking accuracy and maintains the pump flow within an approximately physiological range of 1–4 L/min under varying operating conditions. The proposed controller also exhibits improved adaptability compared with the open-loop LVAD system.

Keywords: LVAD, the cardiovascular system, control parameter, neural network, fuzzy.

1. Introduction

Heart failure (HF) is one of the most prevalent cardiovascular diseases worldwide and is associated with substantial morbidity and mortality [1]. Heart transplantation remains the established treatment for patients with end-stage HF. However, its widespread application is limited by the complexity of the surgical procedure, the shortage of suitable donors, and the increasing prevalence of advanced HF [2], [3]. A left ventricular assist device (LVAD) provides an alternative therapeutic option for patients with advanced HF. It can be used as a bridge to transplantation (BTT) while a patient awaits heart transplantation or as destination therapy (DT) for patients who are not candidates for transplantation [4], [5]. LVAD therapy provides continuous circulatory support by implanting a mechanical pump that assists blood flow from the left ventricle to the aorta. The device helps maintain adequate systemic blood flow and reduces the workload imposed on the weakened ventricle. However, LVADs are often operated at a constant rotational speed, which may result in inadequate blood flow and increase the risk of adverse events, such as ventricular suction and pulmonary congestion, particularly under changing physiological conditions [7]. Therefore, effective LVAD speed regulation is essential to accommodate variations in the patient's physiological state and activity level while maintaining adequate blood flow and avoiding potentially harmful operating conditions. The researchers also sought to address the problem of controlling LVADs. According to Jeongeun Son et al. [8] the integral (I) feedback controller relies on a reference value for pulsatility and continuously adjusts the pump speed to ensure an adequate blood flow rate that meets the body's needs under various operational and physiological conditions. V.C.A. Ko et al.[9] proposed a Centralized Multi-Objective Model Predictive Control (CMO-MPC) for Speed regulation of dual LVADs as a Biventricular Assist Device (BiVAD) system. The controller aims to regulate pump flow according to the Frank-Starling mechanism. This controller relies heavily on pressure and flow sensors to predict future conditions and prevent problems from occurring. Jeongeun Son et al. [10] proposed a model-free adaptive controller (MFAC), characterized by its ability to adjust pump speed in real time without the need for an accurate mathematical model of the cardiovascular system, while taking into account the baroreflex mechanism, which led to improved hemodynamic stability and response to changing blood demand. Although several control strategies have been developed for LVAD speed and flow regulation, existing approaches may rely on accurate physiological measurements, patient-specific models, or computationally intensive control schemes. Model-free approaches can reduce the dependence on an accurate cardiovascular model. However, maintaining stable pump-speed regulation under nonlinear cardiovascular dynamics and changing systemic vascular resistance remains challenging. In addition, the integration of neural-network-based PID control with fuzzy gain tuning for LVAD speed regulation has received limited attention. Therefore, there is a need for a control framework that combines the model-free characteristics of neural-network-based PID control with the flexibility of fuzzy logic to improve controller parameter adjustment under varying physiological conditions. The main contribution of this study is the development of a fuzzy-integrated Neural- PID control framework for LVAD pump-speed regulation within a nonlinear lumped-parameter CVS model. The proposed framework combines a neural-network-based PID structure, which processes the current and delayed speed-tracking errors to generate the proportional, integral, and derivative control components, with a fuzzy inference mechanism for controller-parameter tuning. The proposed controller is evaluated under variations in systemic vascular resistance to examine its ability to maintain stable pump-speed regulation and appropriate pump-flow behavior under changing cardiovascular operating conditions. The effectiveness of the proposed control framework is further assessed by comparing the controlled LVAD response with constant-speed operation. The paper is organized as follows. Section 2 presents the mathematical models of the CVS and the LVAD. Section 3 describes in detail the proposed controller design based on a neural network and fuzzy scheme. Section 4 presents and analyzes the simulation results. Finally, Sections 5 and 6 present the discussion and conclusions, respectively.

2. Mathematical model of the CVS and LVAD

The cardiovascular system (CVS) is a complex and dynamic system comprising numerous variables that describe a patient's physiological condition [11], [12]. It consists primarily of the heart and blood vessels. Its primary function is to receive oxygen-depleted blood from the body and return it to the lungs, where it is oxygenated. The oxygen-rich blood is then returned to the heart, which pumps it to all parts of the body. Each side of the heart consists of two chambers: an atrium and a ventricle [13], [14].

A **lumped-parameter model** was utilized to simplify the design and analysis of the cardiovascular system [3], [15], [16], [17]. The model represents the major components of the circulatory system using equivalent elements based on the **Windkessel model** [12], [18], thereby providing a more tractable mathematical representation of the physiological system. "Fig. 1," illustrates the equivalent electrical circuit used to represent the cardiovascular system incorporating an LVAD [19]. In this electrical analogy, the resistance, elasticity, and inertia of the blood vessels and blood flow are represented by equivalent circuit elements, namely resistance, capacitance, and inductance, respectively. Table 1 presents the electrical equivalents of the lumped-parameter model and their corresponding physiological variables [16].

Table 1. Electrical analogue of the cardiovascular system [20]

Hemodynamic parameters	Circuit parameters
Blood flow resistance	Resistance

Blood flow rate	Current
Blood pressure	Voltage
Vascular compliance	Capacitance
Blood inertia	Inductance

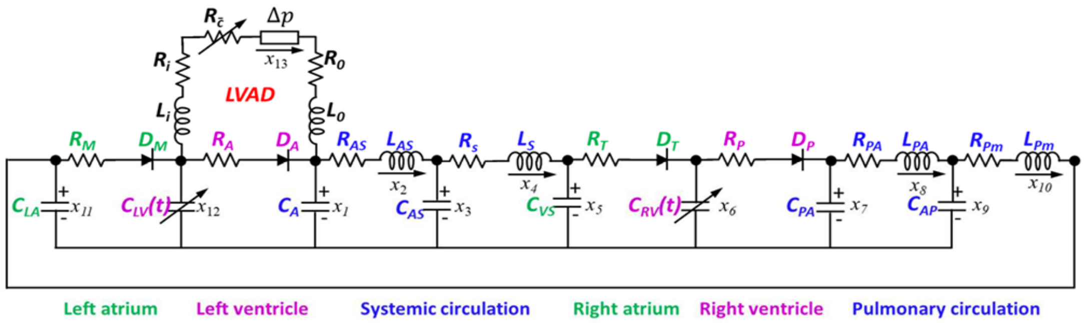

Figure 1. Equivalent electrical circuit representation of the CVS–LVAD model [19]

c(t) reflects the compliance of the left ventricle (LV), as described by "Eq. (1)", while incorporating a time-dependent inverse capacitance function of the left ventricle to illustrate the elastic properties of the heart. "Eq. (2)" can give $E(t)$ elasticity behavior that varies with time in mmHg/ml. This model represents the dynamic relationship between pressure and volume derived from the statement in "Eq. (4)" [19],[21]:

$$c(t) = 1/E(t) \tag{1}$$

$$E(t) = (E_{max} - E_{min})E_n(t_n) + E_{min} \tag{2}$$

$$E_n(t_n) = 1{,}55\left(\frac{\left(\frac{t_n}{0{,}7}\right)^{1{,}9}}{\left(1+\left(\frac{t_n}{0{,}7}\right)^{1{,}9}\right)}\right)\left(\frac{1}{1+\left(\frac{t_n}{1{,}17}\right)^{21{,}9}}\right) \tag{3}$$

$$E(t) = \frac{lvp(t)}{V_{lv(t)} - v_0} \tag{4}$$

$E_n(t_n)$is the normalization function, the so-called "double hill" [14], [21]. $t_n = t/t_{max}$ an $t_{max} = 0.2 + 0.15t_c$, t_c corresponds to the time interval of one cardiac cycle, $t_c = 60/HR$ where HR is the heart rate expressed in beats per minute (bpm) [13]. $Emax$ is the end-systolic pressure, and $Emin$ is the end-diastolic pressure [3], where the v_0 indicates the theoretical ventricular volume as determined by $lvp(t)$=0 [3],[13]. From this previous expression, $lvp(t)$ can evaluate the $lvp(t) = E(t)\left(V_{lv(t)} - V_0\right)$ [12], [22]. The CVS is modelled using a state-space representation, where the model parameters define the system dynamics. The details of each model parameter are available in the literature [19]. The combined modelling of LVAD with CVS is represented by the following nonlinear time-varying differential equation [15]:

$$\dot{x}(t) = A(t)x(t) + B(t)p(x) + cu(t) \tag{5}$$

where x is a variables vector defined in Table 2, A(t), B(t) and c are time-varying matrices, u(t) control variable to the pump speed ω(t), u(t)=ω^2(t), which a controller will tune. The diodes are connected in series with resistors to mimic the behaviors of the heart valves[3],[19]. Valves are used to direct blood flow in a single direction and prevent backward flow [11],[22]. $p(x)$ is a vector designed to replicate the nonlinear dynamics of heart valves [22]. The mathematical expression of the valve is given by “Eq. (6)”, where r(x) is the ramp function:

$$p(x) = \begin{bmatrix} \frac{1}{R_m} r(x_{11} - x_{12}) \\ \frac{1}{R_A} r(x_{12} - x_1) \end{bmatrix}, \; r(x) = \begin{cases} x & if\ x \geq 0 \\ 0 & if\ x < 0 \end{cases} \tag{6}$$

Δp represents the pressure differential across the LVAD pump, calculated as the difference between the inlet and outlet pressures, as defined in [23]. According to “Eq. (7)”:

$$\Delta p = lvp(t) - Aop(t) = \beta_0 x_{13} + \beta_1 \frac{dx13}{dt} + \beta_2 \omega^2 \tag{7}$$

$\beta_0, \beta_1, \beta_2$ which are LVAD-dependent parameters, were set to 0.1707, 0.02177, and 9.9025×10^{-7}, respectively. The phenomenon of suction, which is defined in terms of suction resistance $R_{\bar{C}}$ [23], [24] as follows:

$$R_{\bar{C}}(t) = \begin{cases} \alpha(lvp(t) - lvp(t)_{-suc}) \; if & lvp(t) \leq lvp(t)_{-suc} \\ 0\,, & otherwise \end{cases} \tag{8}$$

Where $\alpha = -3.5\ s/ml$ is the LVAD-dependent parameter, where $lvp(t)_{-suc}$ is the threshold of the LV [23], which is set to 1 mmHg.

Table 2. State variables of the CVS–LVAD model [10],[19]

State variable	Cardiovascular system
x_1	Aortic pressure
x_2	Arterial systemic circulation blood flow
x_3	Arterial systemic pressure
x_4	Venous systemic circulation blood flow
x_5	Right venous-atrial pressure
x_6	Right ventricular pressure
x_7	Pulmonary artery pressure
x_8	Arterial pulmonary circulation blood flow
x_9	Arterial pulmonary pressure
x_{10}	Venous pulmonary circulation blood flow
x_{11}	Left venous-atrial pressure
x_{12}	Left ventricular pressure
x_{13}	LVAD Pump flow

3. The Adaptive Neural Network Controller

The transfer function represents the dynamic behavior of the LVAD $G_p(s)$. “Fig.2” illustrates the general block diagram of the NN-PID controller integrated with the LVAD-CVS model, where the motor torque and pump load torque are denoted by T_e and T_p, respectively. The transfer function of the LVAD is expressed as:

$$G_p(s) = \frac{1}{Js+B} \tag{9}$$

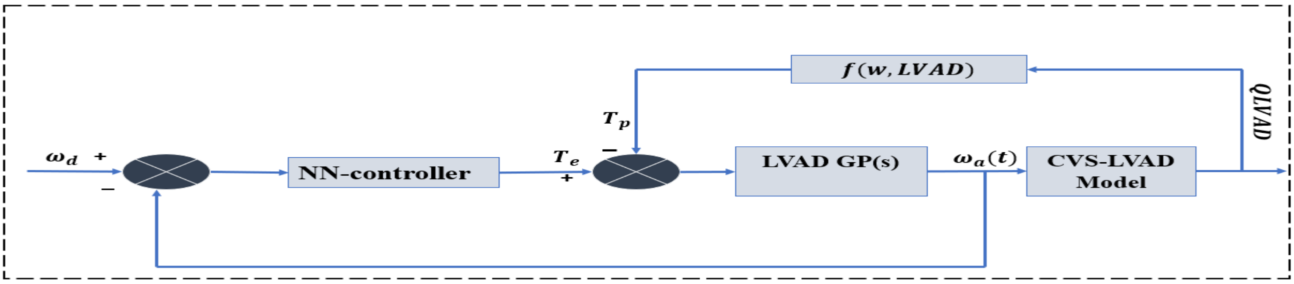

Figure 2. General block diagram of the NN -PID controller with an LVAD-CVS

where $J = 0.916 \times 10^{-6}$ represents the rotor moment of inertia, and $B = 0.660 \times 10^{-6}$ denotes the viscous friction coefficient. The pump load torque is defined as follows:

$$T_p = f(\omega, Q_{LVAD}) = a_0\omega^3 + a_1\omega^2 Q_{LVAD} \tag{10}$$

where $a_0 = 0.738 \times 10^{-12}$and $a_1 = 0.198 \times 10^{-10}$.“Fig. 3,” illustrates the block diagram of the NN-PID controller

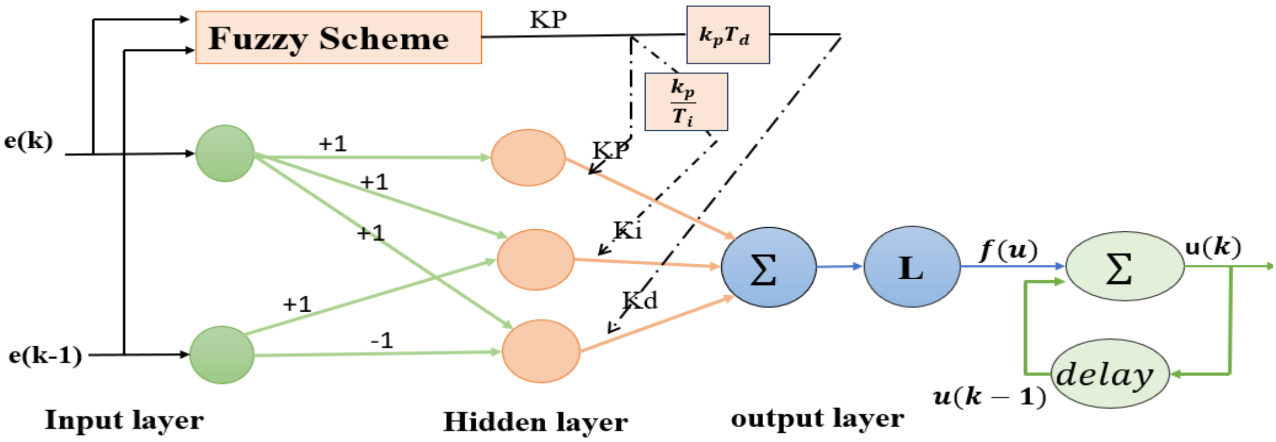

Figure 3. The NN-PID controller

$$kp(k) = f\ fuzzy(e(k), e(k-1)) \tag{11}$$

$$k_i(k) = \frac{k_p}{T_i} \tag{12}$$

$$k_d(k) = k_pT_d = (k_p \times (T_i/4)) \tag{13}$$

$$fu = f(k_pe(k) + k_i(e(k) + e(k-1)) + k_d(e(k) - e(k-1))) \tag{14}$$

$$u(k) = (u(k-1) + fu) \tag{15}$$

Where L is the linear activation function

$$u(k) = k_pe(k) + k_i(e(k) + e(k-1)) + k_d(e(k) - e(k-1)) + u(k-1) \tag{16}$$

The controller implementation is realized using a three-layer computational structure [25]. The input layer receives the current error $e(k)$and the delayed error $e(k-1)$. The hidden layer contains three processing nodes with fixed synaptic weights to extract the discrete proportional, integral, and derivative components. The first node receives $e(k)$ with a unit weight to generate the proportional term. The second node combines $e(k)$ and $e(k-1)$to approximate the discrete integral action. The third node computes the backward difference

$$\Delta e(k) = e(k) - e(k-1) \tag{17}$$

which represents the discrete derivative component. The proposed controller adopts a hybrid fuzzy-neural architecture. “Fig. 4” illustrates the NN-PID controller structure for LVAD-CVS, in which the conventional fixed-gain PID structure is replaced by a modified neural network whose controller parameters are tuned online. The network consists of an input layer receiving the error signal e(k) and its previous value e(k−1), a hidden layer with fixed connection weights (+1, +1, +1, +1, −1) that generate the proportional, integral, and derivative components of the control action, and an output layer that combines these components using time-varying gains $k_p(k)$, $k_i(k)$, and $k_d(k)$. Unlike conventional neural PID structures that adapt all weights through gradient-based learning, the adaptive gains in this network are supplied externally by a fuzzy inference scheme, which maps the error e(k) and the delayed error $e(k-1)$. to an instantaneous proportional gain $k_p(k)$, through a predefined fuzzy rule base. The integral and derivative gains are subsequently derived from $k_p(k)$, through the relations illustrated in “Eq. (12)” ,“Eq. (13)”, respectively.

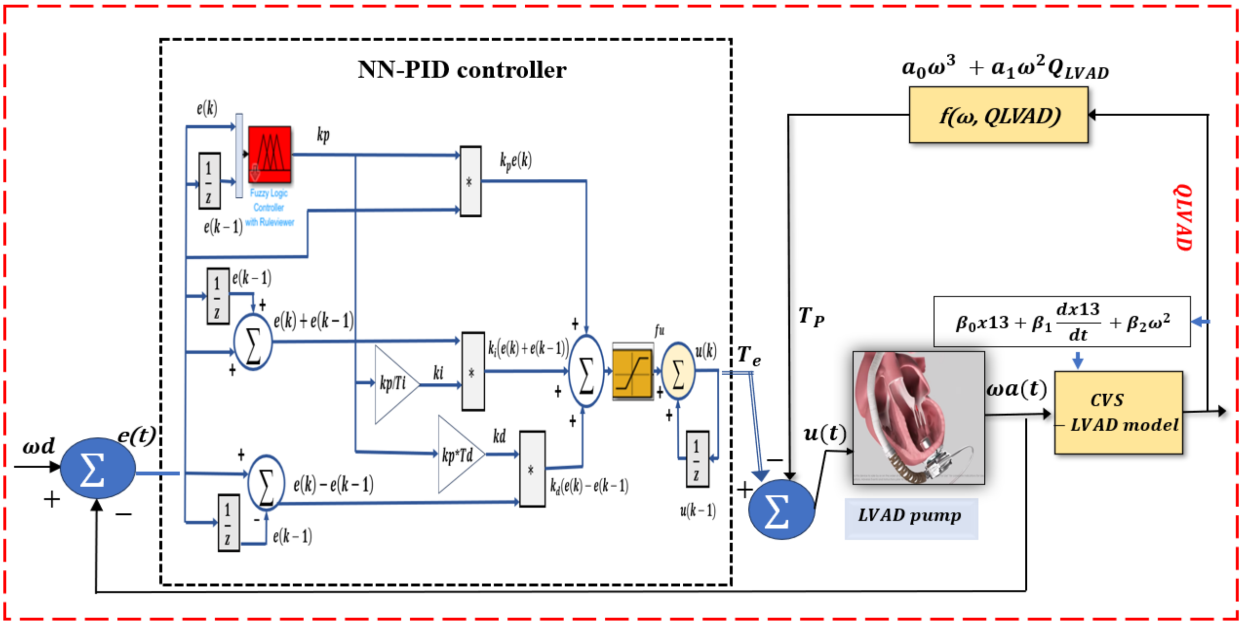

Figure 4. NN-PID controller structure with the LVAD-CVS

The fuzzy scheme used to tune the proportional gain $kp(t)$consists of three main stages: **fuzzification, fuzzy rule base, and defuzzification**

Fuzzification: In this stage, the crisp input signals are converted into their corresponding fuzzy membership values using the predefined triangular membership functions. The fuzzy controller receives two inputs, namely the current tracking error ($e(k)$) and the previous tracking error ($e(k-1)$), and generates one output ($k_p(k)$).

Fuzzy rule base: Based on the selected input membership functions, a set of fuzzy IF–THEN rules is employed to determine the appropriate adjustment of the proportional gain. The fuzzy rules used in the proposed scheme are presented in Table 3. In this table, **N**, **P**, and **Z** denote negative, positive, and zero, respectively. **The**

defuzzification process converts the output of the combined fuzzy system (Fuzzy Inference System) into a crisp numerical value by the following equation:

$$u = \frac{\mu_u(1)*output(1)+\mu_u(2)*output(2)+\cdots+\mu_u(n)*output(n)}{\mu_u(1)+\mu_u(2)+\cdots+\mu_u(n)} \quad (17)$$

Where n represent the number of rules and $\mu_u(n)$ represent the output u membership value. The output ranges from (0 to 0.9) $\times 10^{-4}$

Table 3. Rule table of fuzzy scheme

$\dot{e}_{(t)}$ \ $e_{(t)}$	N	P
N	Z	P
P	N	Z

The speed-tracking error and its rate of variation are continuously monitored. In addition, the neural-network-inspired computational structure facilitates the dynamic extraction of proportional, integral, and derivative error characteristics from the current and delayed tracking-error signals. This adaptive mechanism enhances the flexibility and responsiveness of the proposed controller, allowing it to accommodate rapid hemodynamic variations and the nonlinear operating conditions of the LVAD pump without requiring manual retuning of the PID gains.

4. Simulation Results and Analysis

The performance of the CVS model "Eq. (5)" and the complete controlled LVAD with the CVS model is demonstrated with MATLAB software version R2024a.

4.1 The Simulation Result for CVS To Normal Heart

This section presents simulated hemodynamic responses of the left-sided cardiac circulation based on the mathematical model defined in "Eq. (5)". The model is parameterized to represent a healthy heart. "Fig. 5" illustrates the response of a normal heart at an HR = 75 bpm and an unstressed ventricular volume. "Fig. 5-a" depicts typical values in a healthy CVS profile, highlighting the physiological variation between diastolic and systolic phases. Left ventricular, left atrial, and arterial pressures (mmHg) reflect normal systemic arterial dynamics, and the aortic pressure waveform exhibits a similar physiological range and pattern of fluctuations. "Fig. 5-b" presents the corresponding left ventricular volume (mL), showing consistent filling and ejection patterns. The pressure–volume (PV) relationship is further characterized in "Fig. 5-c". The loop morphology is consistent with normal cardiac function, defined as the difference between end-diastolic volume (EDV) and end-systolic volume (ESV). "Fig. 5-d" demonstrates the total flow from the aorta in a healthy heart.

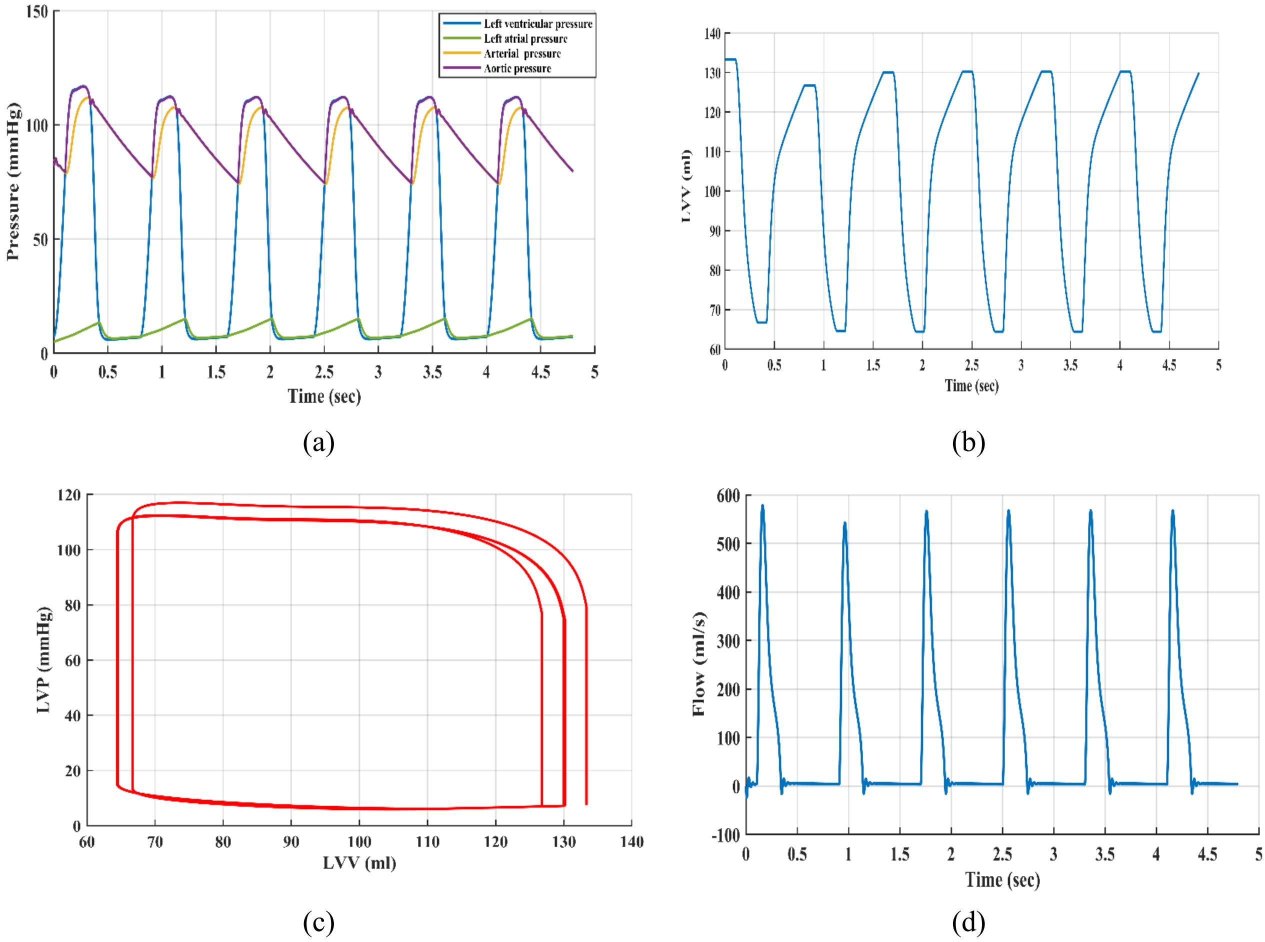

Figure 5. The simulated hemodynamic waveform for a normal heart (a)- Pressure(mmHg) (b)- Volume (mL) (c)- PV- loop (d) -Total flow (mL/s).

4.2 The Simulation Result for the LVAD Device

“Fig. 6” illustrates the LVAD response at constant speed. The flow wave appears regulated, but the curve shows clear irregularity with sharp, recurrent drops in flow rate, indicating a possible suction event in the LVAD. This may result from the pump’s increased speed relative to the left ventricular filling rate, causing the ventricular wall to move toward the pump inlet and reducing the volume of blood the pump draws**.** These disturbances and fluctuations in the waveform are reflected in sudden drops in instantaneous flow values.

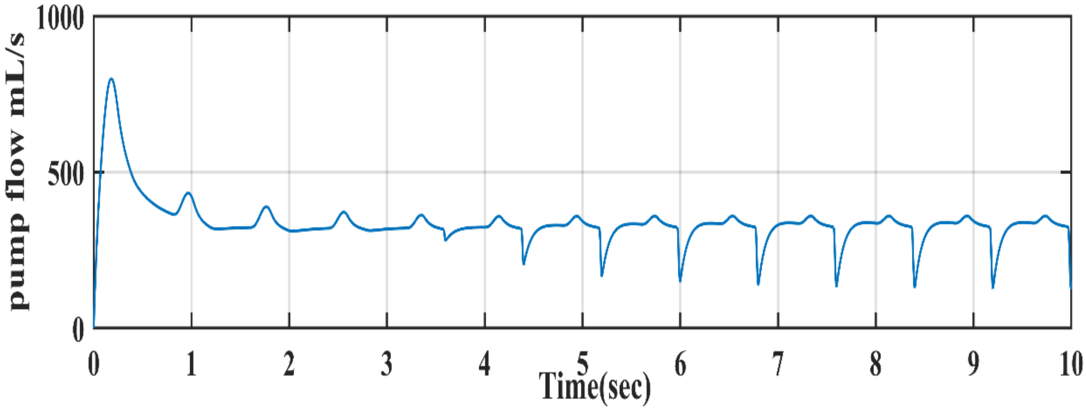

Figure 6. Performance of LVAD flow in mL/s without controller.

4.3 Simulation Results of LVAD Performance Under Suggested Control

An NN–PID controller was applied to the LVAD system. “Fig. 7” illustrates the device's speed and flow responses. The speed signal exhibits a periodic waveform due to the cyclic nature of the CVS connected to the LVAD “Fig. 7-a”. Furthermore, the NN–PID controller effectively suppresses oscillations and compensates for disturbances caused by the nonlinear dynamics of the cardiovascular system, resulting in stable and accurate speed regulation. Fig. “7-b” also shows the flow response of the LVAD pump, where the flow curve appeared relatively smooth and remained within normal physiological limits. No sharp peaks or sudden drops in flow were observed, indicating that no suction phenomenon occurred as a result of excessive blood withdrawal by the pump. Fig. “7-c” shows the variation of the PID gains k_p, k_i, and k_d during the simulation. The results indicate that the LVAD speed reaches its desired value rapidly, resulting in a rapid reduction in the tracking error. Consequently, the PID gains stabilize quickly after the initial transient period and remain nearly constant for the remainder of the simulation. This rapid stabilization of the gains reflects the fast response of the proposed controller. The simulation was conducted at a rotational speed of 12,000 rpm for 60 seconds, allowing for the monitoring of flow behaviors during successive cardiac systole and diastole cycles. The results demonstrate the pump’s stable performance and its ability to adapt to cyclic changes in the CVS while maintaining blood flow.

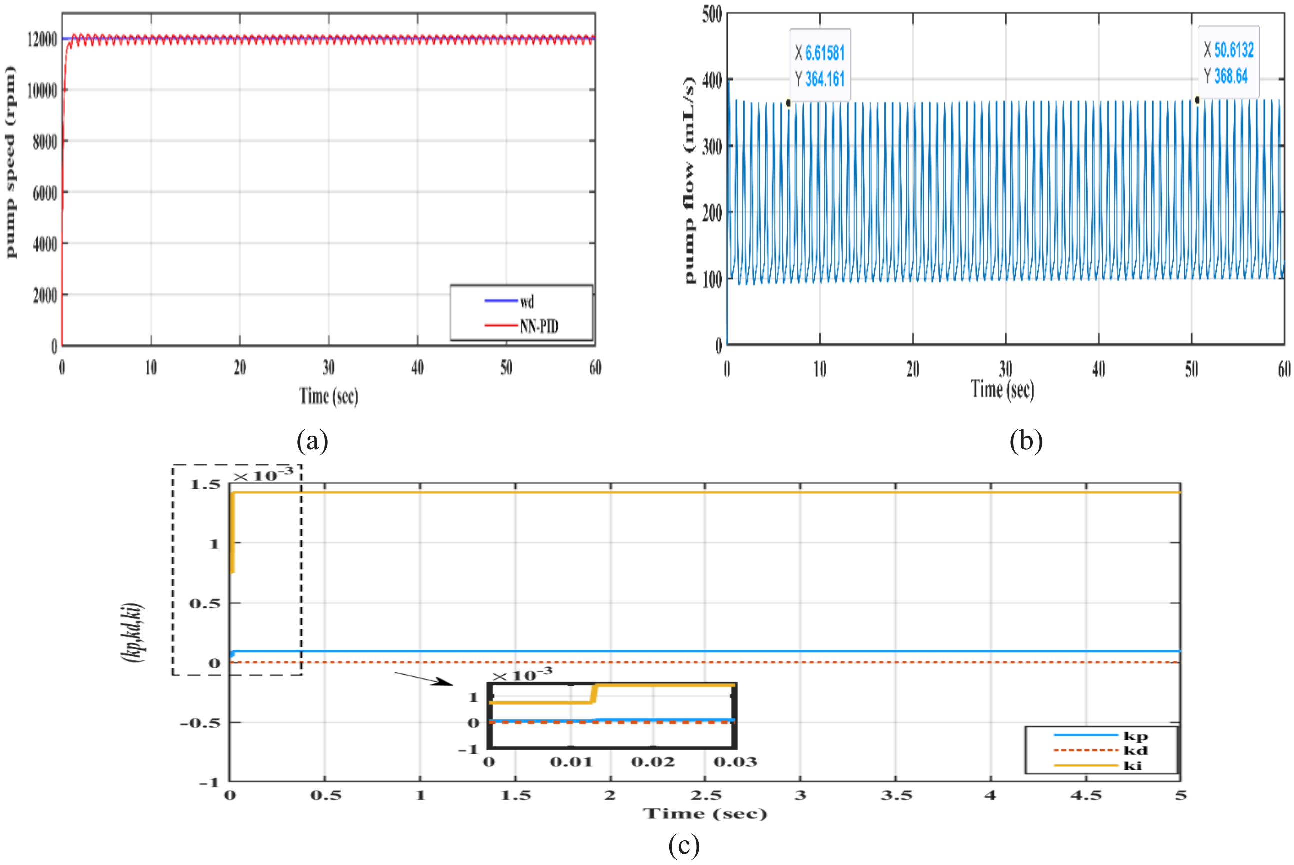

Figure 7. Performance of LVAD under NN-PID controller (a)- Pump speed rpm (b)- Pump flow mL/s (c)- Time variation for controller parameters (k_p, k_i, k_d).

The transient performance of the proposed controller was evaluated in terms of the rise time (t_r), maximum overshoot (Mp), settling time (t_s), and steady-state error (e_{ss}). The results show a rapid response, with a t_r of approximately 0.3 s, indicating that the LVAD speed reaches more than 90% of its final value early in the response. The MP is approximately (1.5- 2) %, demonstrating a small deviation from the desired speed. The t_s based on the ±2% criterion is approximately (1.5) s. After this period, small oscillations of approximately ±120 rpm remain around the e_{ss}. The ess is approximately (0.75) rpm. Overall, these results demonstrate that

The proposed controller provides a fast response. The small residual oscillations in the LVAD speed response can be attributed to the inherent periodic nature of the CVS.

The systemic resistance R_s was adjusted from 1.5 to 1 and then to 0.75 to simulate the gradual decrease in systemic vascular resistance that occurs during the transition from rest to physical activity. Rs represents the resistance encountered by blood as it flows through the systemic circulation and thus reflects the afterload on the heart and the LVAD. “Fig. 8” demonstrates the pump flow with afterloads. Reducing the value of R_s decreased the afterload and facilitated blood flow to the systemic circulation, which resulted in increased LVAD flow. These results indicate that device performance is directly affected by physiological changes.

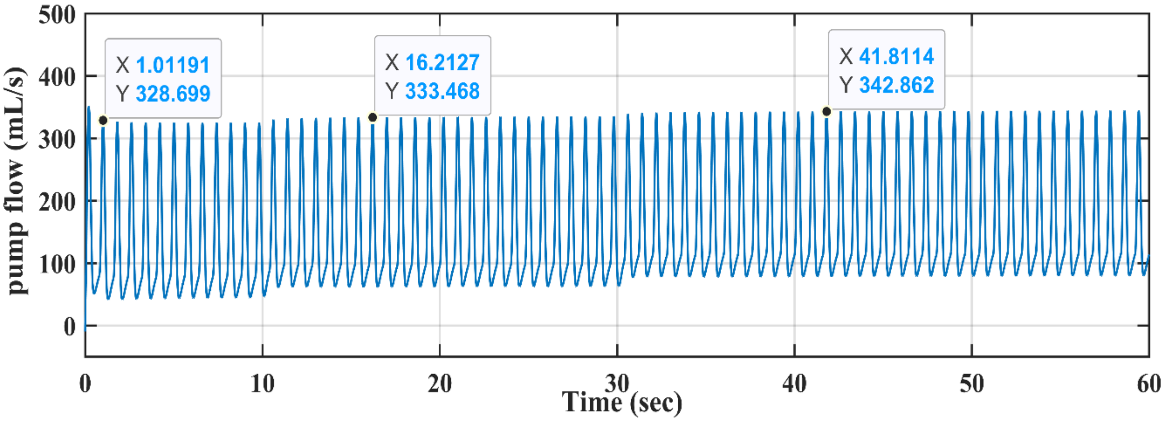

Figure 8. Effect of systemic resistance (R_s) variation on LVAD flow performance

5. Discussion

Regulating LVAD flow and preventing suction remain key challenges in operating the device and integrating it with the patient’s circulatory system. The proposed control strategy aims to regulate LVAD pump speed under varying physiological and hemodynamic conditions, including rest and exercise, while maintaining adequate blood perfusion and avoiding ventricular suction. To achieve this objective, a hybrid control structure combining a neural network and fuzzy logic was developed to improve PID parameter regulation.

The obtained results demonstrate that the proposed controller provides a fast speed response while maintaining an appropriate pump-flow waveform under varying cardiovascular dynamics. This behavior indicates the effectiveness and robustness of the control strategy in handling time-varying hemodynamic conditions. The satisfactory flow response, together with rapid speed tracking, suggests that the controller can compensate effectively for changes in cardiovascular load without causing excessive fluctuations in pump response.

The improved performance can be attributed to the complementary roles of the neural-network and fuzzy-logic components. The neural network reduces the error between the desired reference signal and the actual system response, thereby improving tracking capability. Meanwhile, the fuzzy-logic mechanism updates the PID gains (k_p), (k_i), and (k_d) according to the system error and its variation. These gains are incorporated into the neural-network-based PID control structure, allowing the controller parameters to respond to changes in system dynamics. In contrast to the conventional PID controller, which relies on fixed gains, the proposed approach provides variable control gains that better accommodate changes in cardiovascular load and physiological demand.

This adaptive interaction between the neural network and fuzzy logic contributes to a faster transient response, reduced oscillations, and improved system stability. In particular, maintaining an appropriate pump-flow waveform despite the periodic and nonlinear behavior of the cardiovascular system demonstrates the proposed controller's capability to sustain effective LVAD operation under changing physiological conditions. Therefore, the simulation results support the effectiveness of the proposed hybrid strategy for robust LVAD speed regulation and indicate its potential to maintain adequate pump flow while improving the stability and dynamic response of the overall CVS-LVAD system.

6. Conclusion

This study investigated the use of a mathematical model of the cardiovascular system (CVS) based on the lumped-parameter approach, which provides a simplified and effective representation of the dynamic behavior of the circulatory system through equivalent elements for pressure, flow, resistance, and compliance. The developed model demonstrated a good capability to simulate normal physiological conditions of the heart and reproduce key hemodynamic variables with acceptable accuracy, confirming its suitability as a platform for evaluating the performance of cardiac support systems. A control system combining neural networks and fuzzy logic was also employed to regulate the pump speed and control the blood flow rate according to the patient's physiological requirements. The neural network enhanced the system's ability to adapt to dynamic changes in cardiac conditions, while the fuzzy scheme provided a flexible control mechanism capable of handling the uncertainty and nonlinearity inherent in the cardiovascular system. The simulation results demonstrated that the proposed controller effectively regulated the pump speed and maintained appropriate flow rates within normal physiological limits, while reducing fluctuations and improving the consistency between pump performance and the body's blood flow requirements.

List of abbreviations

Abbreviations	Meaning
$c(t)$	Compliance of the left ventricle
LV	left ventricle
$E(t)$	Elasticity of the left ventricle
E_{max}	End-systolic pressure
E_{min}	End-diastolic pressure
$E_n(t_n)$	The normalization function
t_c	Time interval of one Cardiac cycle
$lvp(t)$	Left ventricular pressure
$V_{lv(t)}$	Volume of the left ventricle
v_0	Theoretical ventricular volume
$A(t)$	Time-varying matrix
$B(t)$	Time-varying matrix
c	Time-varying matrix
$x(t)$	variables vector
$u(t)$	The control variable
$p(x)$	Vector represents the heart valve
R_m	Mitral valve resistance
R_A	Aortic valve resistance
$r(x)$	Ramp function
Δp	Pressure difference
$Aop(t)$	Aortic pressure
ω	Rotational pump speed
$R_{\bar{C}}$	Suction resistance
α	LVAD-dependent parameter

$lvp(t)_{-suc}$	Threshold of the LV
$G_p(s)$	Transfer function
J	Rotor moment of inertia
B	Viscous friction coefficient
T_p	The pump load torque
k_i	Integral gain coefficient
k_p	Proportional gain coefficient
k_d	Derivative gain coefficient
T_i	Integral Time
T_d	Derivative time
$e(k)$	Error
$e(k-1)$	Delayed error
Q_{LVAD}	Pump flow
n	Number of rules
u	Output from fuzzy
HR	Heart rate

Conflicts of Interest

"The authors declare no conflict of interest."

Author Contributions

Ruaa Fadhil developed the research idea, developed the mathematical model, designed and implemented the presented controller, conducted simulations, analyzed the results, and prepared the initial draft of the manuscript. **Ekhlas H. Karam** supervised the research, contributed to the interpretation of the results, carefully reviewed the manuscript scientifically, and approved the final version of it.

Acknowledgments

The authors declare that no specific funding was received for this research

Reference

[1] V. L. Roger, "Epidemiology of Heart Failure: A Contemporary Perspective," *Circulation Research,* vol. 128, no. 10, pp. 1421-1434, 2021, doi: 10.1161/CIRCRESAHA.121.318172.

[2] V. S. Vasudevan, K. Rajagopal, and J. F. Antaki, "Application of mathematical modeling to quantify ventricular contribution following durable left ventricular assist device support," *Applications in Engineering Science,* vol. 11, pp. 100107, 2022, doi: 10.1016/j.apples.2022.100107.

[3] M. Melendo-Viu, D. Dobarro, S. Raposeiras Roubin, C. Llamas Pernas, C. Moliz Cordón, M. Vazquez Lamas, M. Piñón Esteban, M. Á. Varela Martínez, E. Abu Assi, R. Pita Romero, J. J. Legarra Calderón, and A. Íñiguez Romo, "Left Ventricular Assist Device as a Destination Therapy: Current Situation and the Importance of Patient Selection," *Life,* vol. 13, no. 4, p. 1065, 2023, doi: 10.3390/life13041065.

[4] T. D. Cordeiro, D. L. Sousa, I. A. Cestari, and A. M. N. Lima, "A physiological control system for ECG-synchronized pulsatile pediatric ventricular assist devices," *Biomedical Signal Processing and Control,* vol. 57, p. 101752, 2020, doi: 10.1016/j.bspc.2019.101752.

[5] L. G. E. Cox, S. Loerakker, M. C. M. Rutten, B. A. J. M. De Mol, and F. N. Van De Vosse, "A mathematical model to evaluate control strategies for mechanical circulatory support," *Artificial Organs,* vol. 33, no. 8, pp. 593-603, 2009, doi: 10.1111/j.1525-1594.2009.00755.x.

[6] M. Yuzefpolskaya *et al.*, "The Society of Thoracic Surgeons Intermacs 2022 Annual Report: Focus on the 2018 Heart Transplant Allocation System," *The Annals of Thoracic Surgery,* vol. 115, no. 2, pp. 311-327, 2023, doi: 10.1016/j.athoracsur.2022.11.023.

[7] M. Fetanat, M. Stevens, C. Hayward, and N. H. Lovell, "A Sensorless Control System for an Implantable Heart Pump Using a Real-Time Deep Convolutional Neural Network," *IEEE Transactions on Biomedical Engineering,* vol. 68, no. 10, pp. 3029-3038, 2021, doi: 10.1109/TBME.2021.3061405.

[8] J. Son, D. Du, and Y. Du, "Feedback Control of Rotary Blood Pump for Preventing Left Ventricular Suction," in Proc. 2019 American Control Conference (ACC), Philadelphia, PA, USA, 2019, pp. 5426-5430.

[9] V. C. A. Koh *et al.*, "A centralized multi-objective model predictive control for a biventricular assist device: An in silico evaluation," *Biomedical Signal Processing and Control,* vol. 49, pp. 137-148, 2019, doi: 10.1016/j.bspc.2018.10.021.

[10] J. Son and Y. Du, "Model-Free Adaptive Control of the Failing Heart Managed by Mechanical Supporting Devices," in *IFAC-PapersOnLine,* 2022, pp. 750-755, doi: 10.1016/j.ifacol.2022.07.534.

[11] M. Iscan and A. Yesildirek, "Modeling Transient Cardiovascular Hemodynamics with Physiological Conscious Autoencoder," *IEEE Access,* vol. 11, pp. 111909-111926, 2023, doi: 10.1109/ACCESS.2023.3322943.

[12] J. E. Traver *et al.*, "Cardiovascular Circulatory System and Left Carotid Model: A Fractional Approach to Disease Modeling," *Fractal and Fractional,* vol. 6, no. 2, p. 64, 2022, doi: 10.3390/fractalfract6020064.

[13] M. Khaledi, M. Dehghani, R. Abolpour, and M. Mohammadi, "Controller Design for Left Ventricular Assist Devices in Patients with Heart Failure," in Proc. 2020 27th National and 5th International Iranian Conference on Biomedical Engineering (ICBME), Tehran, Iran, 2020, pp. 326-332, doi: 10.1109/ICBME51989.2020.9319420.

[14] Y. S. Kim, E.-H. Kim, H.-G. Kim, E. B. Shim, K.-S. Song, and K. M. Lim, "Mathematical analysis of the effects of valvular regurgitation on the pumping efficacy of continuous and pulsatile left ventricular assist devices," Integrative Medicine Research, vol. 5, no. 1, pp. 22-29, 2016, doi: 10.1016/j.imr.2016.01.001.

[15] G. Faragallah, Y. Wang, E. Divo, and M. A. Simaan, "A New Current-Based Control Model of the Combined Cardiovascular and Rotary Left Ventricular Assist Device," in *Proc. 2011 American Control Conference (ACC),* San Francisco, CA, USA, 2011, pp. 4775-4780, doi: 10.1109/ACC.2011.5990641.

[16] V. S. Vasudevan, K. Rajagopal, and J. F. Antaki, "Application of mathematical modeling to quantify ventricular contribution following durable left ventricular assist device support," *Applications in Engineering Science,* vol. 11, p. 100107, 2022, doi: 10.1016/j.apples.2022.100107.

[17] K. Gu, Y. Chang, B. Gao, Y. Liu, Z. Zhang, and F. Wan, "Lumped parameter model for heart failure with novel regulating mechanisms of peripheral resistance and vascular compliance," *ASAIO Journal,* vol. 58, no. 3, pp. 223-231, 2012, doi: 10.1097/MAT.0b013e31824ab695.

[18] N. Westerhof, J. W. Lankhaar, and B. E. Westerhof, "The arterial Windkessel," *Medical Engineering & Physics,* vol. 31, no. 2, pp. 131-141, 2009, doi: 10.1007/s11517-008-0359-2.

[19] J. Son, D. Du, and Y. Du, "Modelling and control of a failing heart managed by a left ventricular assist device," *Biocybernetics and Biomedical Engineering,* vol. 40, no. 1, pp. 559-573, 2020, doi: 10.1016/j.bbe.2020.01.014.

[20] X. Liu *et al.*, "Development of a Lumped Parameter Model of Human Whole Body Circulatory Loop," *IEEE Access,* vol. 12, pp. 188505-188518, 2024, doi: 10.1109/ACCESS.2024.3491112.

[21] Y. Bao, T. Jing, W. Ru, and L. Zhou, "Pulsatile Physiological Control of Blood Pump-Cardiovascular System Based on Feedforward Compensation," *Micromachines,* vol. 16, no. 6, p. 664, 2025, doi: 10.3390/mi16060664.

[22] S. Wolpe, "A Heart Valve is a One-Way Valve that Allows Blood to Flow in One Direction through the Chambers of the Heart," *Interventional Cardiology Journal,* vol. 9, no. 2, p. 20, 2023, doi: 10.21767/2471-8157.9.02.20.

[23] L. F. V. Silva and T. D. Cordeiro, "A variable gain physiological controller for a rotary left ventricular assist device," in *Proc. 2021 43rd Annual International Conference of the IEEE Engineering in Medicine & Biology Society (EMBC),* Virtual Conference, 2021, pp. 5606-5609, doi: 10.1109/EMBC46164.2021.9630835.

[24] J. Son, D. Du, and Y. Du, "Modelling and control of a failing heart managed by a left ventricular assist device," *Biocybernetics and Biomedical Engineering,* vol. 40, no. 1, pp. 559-573, 2020, doi: 10.1016/j.bbe.2020.01.014.

[25] W. T. J. Al-Rubaye, A. S. Al-Araji, and H. A. Dhahad, "An Adaptive Digital Neural Network-Like-PID Control Law Design for Fuel Cell System Based on FPGA Technique," *Journal of Engineering,* vol. 26, no. 9, pp. 24-44, 2020, doi: 10.31026/j.eng.2020.09.03.